

Surface Stiffness Estimation using Active Strobe Imager

Taiki Yamaguchi

Graduate School of Engineering Science, Osaka University, 1-3, Machikaneyama-cho, Osaka, Japan

Kensuke Harada

Graduate School of Engineering Science, Osaka University, 1-3, Machikaneyama-cho, Osaka, Japan

Email: {yamaguchi@hlab, harada@}.sys.es.osaka-u.ac.jp

Kouji Mizoue

Mizoue Project Japan, 305-1 Takagi-cho, Fuchu-city,726-0013, Hiroshima, Japan

Makoto Kaneko

Graduate School of Engineering Science, Osaka University, 1-3, Machikaneyama-cho, Osaka, Japan

Email: {president, mkaneko}@mizoueproject.com

Abstract

In this paper, we propose a method for estimating mechanical impedance of surface like skin using an Active Strobe Imager (ASI). ASI has the capability to non-contactly excite the target surface using an air jet flow, and to qualitatively observe traveling waves through strobe illumination. On the other hand, this paper shows that the surface impedance parameter can be estimated without contacting the target surface along with the visualization through ASI. We solve two problems: one is the inverse problem and the other is the forward problem. In the inverse problem, we estimate the spring constant of the target using information obtained from the measurement data. In the forward problem, we determine the surface displacement from the applied force, we compared the obtained displacement from the measurement data, demonstrating that the spring constants were correctly estimated.

Keywords: Spring-constant, Non-contact, Estimation.

1. Introduction

The mechanical impedance of materials is recognized as a crucial parameter characterizing the subject. For instance, in the case of soft biological tissues, such as internal organs, skin, and muscles, the mechanical impedance serves as essential biomarkers in medical diagnostics.[1][2][3][4][5] Given this context, numerous foundational studies propose the mechanization of palpation performed by physicians for medical diagnostics on soft matter.[6][7][8][9][10][11][12] However, most of these approaches predominantly rely on contact-based estimations, rendering them unsuitable for subjects where direct contact is undesirable, due to concerns such as infection or tissue damage.

In response to this issue, Kaneko et al. have proposed the Active Strobe Imager (ASI) as a non-contact method for estimating the mechanical impedance. [13] The ASI incorporates periodically controlled air jets and a stroboscope, as shown in Figure 1. It allows for the observation of the propagating waves induced by the air jet on the target, enabling the qualitative assessment of its stiffness without direct contact. Given these capabilities, qualitative estimation of stiffness in soft biological tissues has been widely conducted. Tanaka et al.[14] then irradiated the skin surface with a slid laser beam, measuring the observed waves generated on the skin surface using a high-speed camera, providing finer observations

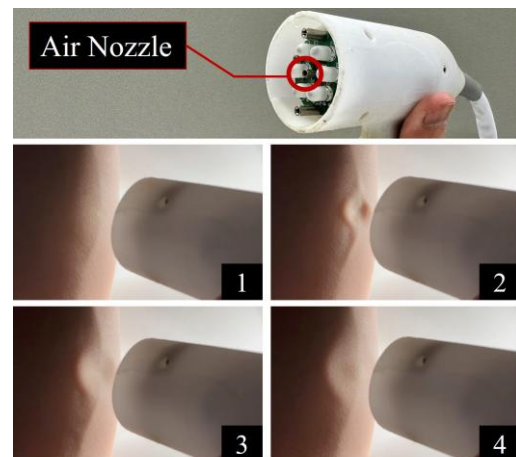


Fig 1. Waves propagating on the skin surface created by periodic air jet flows.

and assessments when air jetting was performed. In addition, Kawahara et al.[15] proposed a method to visually detect relatively rigid areas compared to the surrounding tissues by applying fluidic forces to the measurement target. Funai et al.[16] proposed design parameters clearly visualizing the movements of rapidly vibrating objects by appropriately setting stroboscopic illumination. Thus, attempts to use ASI for visually understanding the motion of the target and qualitatively

assessing stiffness have been widely made. However, quantitative evaluations of measurement targets using ASI have not been investigated so far.[17]

In this paper, we propose a method to utilize strobe illumination to quantitatively estimating the surface mechanical impedance. We solve two problems, i.e., the inverse and forward problems, i.e., We first model the dynamics of elastic membrane by using a series of linear springs. In the inverse problem, by estimating the force applied by the air jet by identifying the relation between the pressure of the air jet and force obtained from FSR, we probe that the spring constant can be identified. On the other hand, in the forward problem, we confirm that the estimated spring constant well matches the experimental result. In the forward problem, the analytical solution can be obtained in the explicit form.

In the subsequent chapters, we will summarize the measurement instruments and visualization techniques in Chapter 2, discuss the estimation methods for spring constants in Chapter 3, compile the measurement data in Chapter 4, and conclude in Chapter 5, 6.

2. Measurement Environment & Visualization Principles

To estimate the spring constant of the rubber membrane using ASI, it is necessary to have data on the applied force and displacement. Here, we will explain the equipment used to measure the force of the air jet generated from ASI and the displacement of the rubber membrane. Additionally, we will demonstrate the changes in the rubber membrane by visualizing the characteristics of the measured vibrations using stroboscopic illumination. Major headings should be typeset in boldface with the first letter of important words capitalized.

2.1. Force measurement device

Figure 2 depicts the equipment used to measure the force of the air jet generated by ASI. A Force Sensing Resistor (FSR) is utilized as the force sensor, which can measure the periodic force of the air jet by applying it to the sensor.

2.2. Instrumentation for Displacement Measurement

Next, figure 3 illustrates a displacement measurement apparatus. This apparatus is equipped with ASI, a rubber membrane, a laser displacement sensor, a camera, and a stroboscope. This device serves two functions: firstly, it measures the displacement of the rubber membrane, and secondly, it visualizes the vibrations of the rubber membrane induced by periodic air jetting.

2.3. Visualization Principles

We employed strobe effect for visualization. This method allows us to visualize the vibrations of the rubber membrane, which are too rapid to be observed by the naked eye due to ASI air jet, by precisely timing the



Fig 2. Force measurement instrument utilizing a force sensing register.

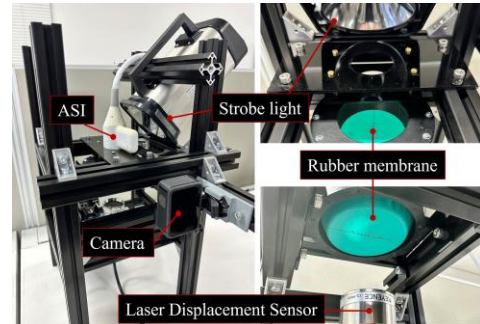


Fig 3. Displacement measurement device capable of measuring the displacement of a rubber membrane and visualizing progressive waves.

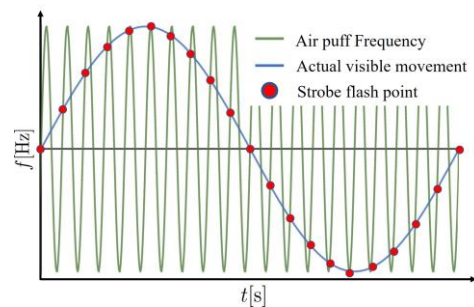


Fig 4. Waves propagating on the skin surface created by periodic air jet flows.

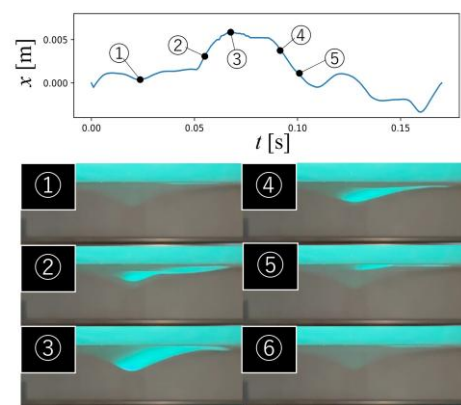


Fig 5. Visualization principle generated by periodic air jetting and stroboscope illumination.

strobe illumination. [figure 4](#) depicts a graph illustrating the timing of air jet and strobe illumination. The green curve represents the frequency of the air jet, while the red dots indicate the strobe illumination points. By appropriately adjusting the strobe illumination frequency relative to the frequency of the air jet, we utilize a mechanism that allows us to observe the solid blue line enabling visualization.

[Figure 5](#) illustrates a graph depicting the displacement of the rubber membrane subjected to excitation by ASI, as measured by a laser displacement sensor, along with its visualization of vibrations. In this experiment, the frequency of air jetting was set to 60 Hz with a 50% duty factor, and the stroboscope illumination frequency was set to 61 Hz. The displacement information measured by the laser displacement sensor is represented by the solid blue line. As observed in the visualized images, the rubber membrane initially undergoes depression, followed by a vibration pattern where the membrane returns when the electromagnetic valve closes.

3. Estimation of spring constant

In this section, we will elucidate a model for estimating spring constants based on the data of force and displacement measured using the instruments discussed in Chapter 2. Specifically, we will consider models for a thin rubber membrane, one employing two springs and another employing three springs and we will estimate the spring constants for each model using the ASI and compare the results.

3.1. Two-Spring Model

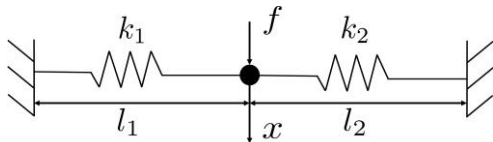


Fig 6. Overview diagram of the Two-Spring Model.

Estimate the spring constants of the rubber membrane, we considered the system shown in [figure 6](#) and formulated the motion equation, represented as equation 1, to describe the response to the applied forces. Here, k_1 and k_2 represent the spring constants, l_1 and l_2 denote the distances from the fixed ends of the springs to the measurement points, f represents the force of the air jet, and x represents the displacement of the rubber membrane. Additionally, both the force f and the displacement x are continuously measured until the end of the measurement period, denoted as t_{end} . Furthermore, we express equation 1 in the form of a state equation using equation 2.

$$f(t) = 2k_1 \frac{x^3(t)}{l_1^2} + 2k_2 \frac{x^3(t)}{l_2^2}, \quad \forall t \in [0, t_{end}] \quad (1)$$

$$\begin{bmatrix} f(t) \\ \vdots \\ f(t_{end}) \end{bmatrix} = \begin{bmatrix} k_1 \\ k_2 \end{bmatrix} \begin{bmatrix} \frac{2x^3(t)}{l_1^2} & \frac{2x^3(t)}{l_2^2} \\ \vdots & \vdots \\ \frac{2x^3(t_{end})}{l_1^2} & \frac{2x^3(t_{end})}{l_2^2} \end{bmatrix} \quad (2)$$

Next here, we consider an inverse problem to estimate the spring constants. If the time-series force $f(t)$ and displacement $x(t)$ as depicted in the equation are known, the spring constants k_1 and k_2 can be expressed using the generalized inverse of the displacement matrix, as shown in the following equation 3 (where "#" denotes the generalized inverse). Additionally, in the current measurement environment where the laser displacement sensor provides measurements at only one point, we assume that the force f applied by air injection is ideally applied from the injection nozzle to the rubber membrane. Therefore, it can be represented as the product of the nozzle cross-sectional area S and air pressure P , as given in equation 4.

$$\begin{bmatrix} k_1 \\ k_2 \end{bmatrix} = \begin{bmatrix} \frac{2x^3(t)}{l_1^2} & \dots & \frac{2x^3(t_{end})}{l_1^2} \\ \frac{2x^3(t)}{l_2^2} & \dots & \frac{2x^3(t_{end})}{l_2^2} \end{bmatrix}^{\#} \begin{bmatrix} f(t) \\ \vdots \\ f(t_{end}) \end{bmatrix} \quad (3)$$

$$f(t) = SP \quad (4)$$

On the other hand, in order to compare the displacement with the actual measured value, it is necessary to find an equation that explains the displacement based on the relationship between the estimated spring constants k_1 and k_2 obtained in Equation 3 and the force. Here, the comparison is made from Equation 5, where Equation 1 is obtained analytically for displacement x .

$$x = \left(\frac{f}{K} \right)^{\frac{1}{3}} \quad (5)$$

$$K = 2 \left(\frac{k_1}{l_1^2} + \frac{k_2}{l_2^2} \right)$$

3.2. Three-Spring Model

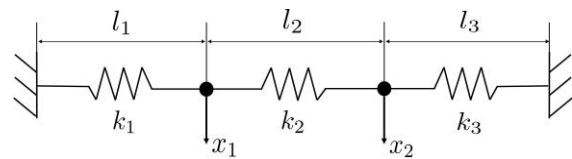


Fig 7. Overview diagram of the Three-Spring Model.

Furthermore, consider a model in which the rubber membrane is described by three springs. As shown in [figure 7](#), unlike the previously mentioned two-spring model, adding more springs results in two points where forces are applied. To simplify the problem, we will proceed with estimating the spring constants under the condition that the force is applied to either the x_1 or x_2 side only. Therefore, we provide the equations of motion for the model where force is applied to the x_1 side, as shown in [Figure. 8a](#)), in equations 6a and 6b, and the equations of motion for the model where force is applied

to the x_2 side, as shown in figure 8b, in equations 7a and 7b. Furthermore, the force f here is given in the same manner as in equation 4 for the two-spring model.

$$\begin{cases} 2k_{11} \frac{x_1^3(t)}{l_1^2} + 2k_{12} \frac{(x_1(t) - x_2(t))^3}{l_2^2} = f(t) \\ -2k_{21} \frac{(x_1(t) - x_2(t))^3}{l_2^2} + 2k_{22} \frac{x_2^3(t)}{l_3^2} = 0 \end{cases} \quad (6a) \quad (6b)$$

$$\begin{cases} 2k_{11} \frac{x_1^3(t)}{l_1^2} + 2k_{12} \frac{(x_1(t) - x_2(t))^3}{l_2^2} = 0 \\ -2k_{21} \frac{(x_1(t) - x_2(t))^3}{l_2^2} + 2k_{22} \frac{x_2^3(t)}{l_3^2} = f(t) \end{cases} \quad (7a) \quad (7b)$$

Here, k represent spring constants, while l_1 , l_2 , and l_3 denote the distances to each measurement point. We have set up the force $f(t)$ and displacements $x_1(t)$ and $x_2(t)$ as measurement data obtained over time. Consider the problem of estimating the spring constant by inverse problem of Equations 6 and 7 in conjunction. As mentioned in the introduction, when a force is applied to one side, no force is applied to the other side. If we wish to estimate the spring constants k_{12} , k_{22} using only the two equations in Equation 6, there is a problem that k_{22} cannot be obtained because no force is applied in Equation 6b. Therefore, we focus on Equations 6a and 7b, in which a force is applied, and estimate the respective spring constants from the equations of state shown in Equation 8.

$$\mathbf{f} = \mathbf{k} \mathbf{x} \quad (8)$$

$$\mathbf{f} = \begin{cases} \begin{bmatrix} f \\ 0 \end{bmatrix}, & \text{if a force is applied to } x_1, \\ & \text{and this results in } f_2 = 0. \\ \begin{bmatrix} 0 \\ f \end{bmatrix}, & \text{if a force is applied to } x_2, \\ & \text{and this results in } f_1 = 0. \end{cases}$$

$$\mathbf{k} = \begin{bmatrix} k_{11} & k_{12} \\ k_{21} & k_{22} \end{bmatrix} \quad \mathbf{x} = \begin{bmatrix} \frac{2x_1^3(t)}{l_1^2} & \frac{-2(x_1(t) - x_2(t))^3}{l_2^2} \\ \frac{2(x_1(t) - x_2(t))^3}{l_2^2} & \frac{2x_2^3(t)}{l_3^2} \end{bmatrix}$$

Therefore, from Equation 8 we obtain Equation 9 for estimating the spring constant.

$$\mathbf{k} = \mathbf{x}^\# \mathbf{f} \quad (9)$$

Next, as in the two-spring model, consider the forward problem of finding the displacements x_1 and x_2 from the estimated spring constants \mathbf{k} , and force \mathbf{f} .

First, consider the forward problem shown in figure 8a. Here, the analytical displacements x_1 and x_2 are calculated by solving the simultaneous equations in Equation 6. First, Equation 6b is computed for x_2 to obtain Equation 10.

$$x_2 = Qx_1 \quad (10)$$

$$Q = \frac{1}{1 + A} \quad A = \left(\frac{k_{21} l_3^2}{k_{22} l_2^2} \right)^{\frac{1}{3}}$$

Next, substitute Equation 10 into x_2 in Equation 6a to obtain the analytical solution for x_1 .

$$x_1 = \left(\frac{f}{W} \right)^{\frac{1}{3}} \quad (11)$$

$$W = 2 \left(\frac{k_{11}}{l_1^2} + \frac{k_{12}}{l_2^2} (1 - Q)^3 \right)$$

We will similarly seek an analytical solution for x_2 . Since we already have the expression for x_1 from Equation 11, we can substitute it into Equation 6b and solve for x_2 as a solution to a cubic equation. For brevity, we will only present the coefficients of the cubic equation here.

$$\alpha x_2^3 - 6\beta \left(\frac{f}{W} \right)^{\frac{1}{3}} x_2^2 + 6\beta \left(\frac{f}{W} \right)^{\frac{2}{3}} x_2 - 2\beta \left(\frac{f}{W} \right) = 0 \quad (12)$$

$$\alpha = 2 \left(\frac{k_{21}}{l_2^2} + \frac{k_{22}}{l_3^2} \right) \quad \beta = \frac{k_{21}}{l_2^2}$$

Similarly, we seek to obtain the analytical solution for the case depicted in figure 8b. We begin by focusing on Equation 7a and solving for x_1 , thereby deriving Equation 13.

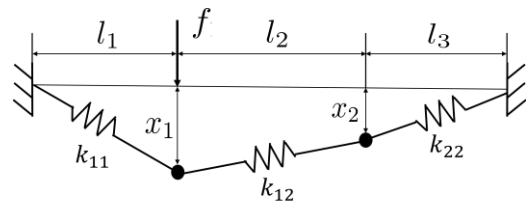
$$x_1 = Sx_2 \quad (13)$$

$$P = \frac{S}{1 + S} \quad S = \left(\frac{k_{12} l_1^2}{k_{11} l_2^2} \right)^{\frac{1}{3}}$$

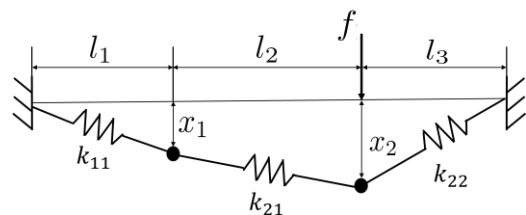
We will now substitute equation 13 into equation 7b to obtain the expression for x_2 .

$$x_2 = \left(\frac{f}{T} \right)^{\frac{1}{3}} \quad (14)$$

$$T = 2 \left(-\frac{k_{21}}{l_2^2} (P - 1)^3 + \frac{k_{22}}{l_3^2} \right)$$



(a) When force is applied to x_1 side.



(b) When force is applied to x_2 side.

Fig 8. Overview diagram of the Three-Spring Model.

Thereafter, similar to Equation 12, Equation 14 is substituted into Equation 7a, and the coefficients of the cubic equation are summarized.

$$\gamma x_1^3 - 6\delta \left(\frac{f}{T}\right)^{\frac{1}{3}} x_1^2 + 6\delta \left(\frac{f}{T}\right)^{\frac{2}{3}} x_1 - 2\delta \left(\frac{f}{T}\right) = 0 \quad (15)$$

$$\gamma = 2 \left(\frac{k_{11}}{l_1^2} + \frac{k_{12}}{l_2^2} \right) \quad \delta = \frac{k_{12}}{l_2^2}$$

4. Experimental Measurement

In this section, we conducted experiments to measure force and displacement to estimate the spring constants for both the two-spring and three-spring models. We will summarize the results for each of them.

4.1. Measurement of the Three-Spring Model

The displacement and force time series data needed to estimate the two-spring model are shown in figure 9. The distances shown in figure 6, l_1 and l_2 , were both set to l_1 and l_2 as 35×10^{-3} [m]. And ASI duty factor set to 100% for this data, and the magnitude of the force was ideally given as 1.57[N] by Equation 4.

4.2. Measurement of the Three-Spring Model

Figure 10 depicts the waveforms of force and displacement when forces are applied to x_1 , x_2 respectively, as shown in figure. 8a and figure 8b. The distance between measurement points is set as follows: $l_1 = l_3 = 27.5 \times 10^{-3}$ [m] and $l_2 = 15 \times 10^{-3}$ [m]. These waveforms were generated by directing ASI air jet at a duty factor of 100%.

On the other hand, ASI originally measures the target using periodic air jet. Therefore, in figure 11 (Displacement & Force), we measured the displacements, x_1 and x_2 , by subjecting the rubber membrane to forced vibrations using a periodic air jet at 60 Hz with a 50% duty factor. However, there is an issue where the actual waveform of the force applied to the rubber membrane does not drop to zero at a 50% duty factor due to the physical delay in the opening and closing of the electromagnetic valve. To address this issue, we used the force measuring device shown in figure. 2 to measure the actual waveform and based on the duty factor indicated in figure 11 (FSR), we created an ideal rectangular waveform for the force, represented by the orange line.

5. Estimated Results

We will present the results of the spring constants obtained from the inverse problem in figure 12, 13, and 14, as well as the results obtained by solving the forward problem. First, figure. 12 shows the estimation results for a model with two springs, with spring constants estimated as $k_1 = k_2 = 8429.25$ [N/m]. On the other hand, we depict the forward problem solved based on the applied force and estimated spring constants with a red line. At this point, the displacement obtained from the analysis

was $x = 3.84 \times 10^{-3}$ [m]. In contrast, we plotted the results of the measured data with a blue dashed line for comparison. As can be seen from the figure, the estimated displacement value and the measured displacement value match very closely, confirming that the spring constants were correctly estimated.

Next, focus on the results obtained for the model with three springs. In figure 13, these results were obtained by solving the inverse problem using the displacement and force data shown in figure 10. Here, because x_1 and x_2 interact with each other, we did not obtain results similar to the two-spring model. However, it is worth noting that the spring constants at both ends estimated for the two-spring model and the three-spring model when subjected to static forces show very close values.

Furthermore, when comparing the data obtained through the forward problem with the measurement data obtained using a laser displacement sensor, we confirmed that these results also closely match.

Finally, summarize the results obtained from the dynamic force application in figure 14. First, it is evident that the estimated spring constants are considerably lower when compared to the results obtained from the three-spring model subjected to static forces.

Additionally, a significant discrepancy can be observed between the analytically solved displacement values depicted by the red line and the measured displacement values. We attribute this difference to the influence of inertia caused by the periodic application of force, which was not accurately estimated.

However, based on the results from figure 12 and 13, which were obtained under static conditions, it has been demonstrated that in this model, the spring constants can be accurately estimated when subjected to static force application

6. Summary

In this study, we used ASI to measure and quantitatively evaluate a rubber membrane non-contact. Here, we estimated the spring constant from two models for thin rubber membranes and compared them by solving an forward problem using the obtained spring constants. As a result, the proposed model demonstrated accurate estimation under conditions with applied static forces. In the future, we plan to construct even more complex models and continue with the estimation process.

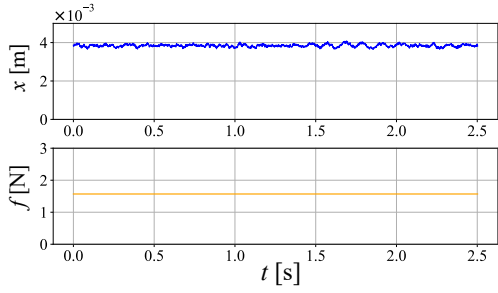


Fig 9. Static measurement data of displacement (blue line) and force

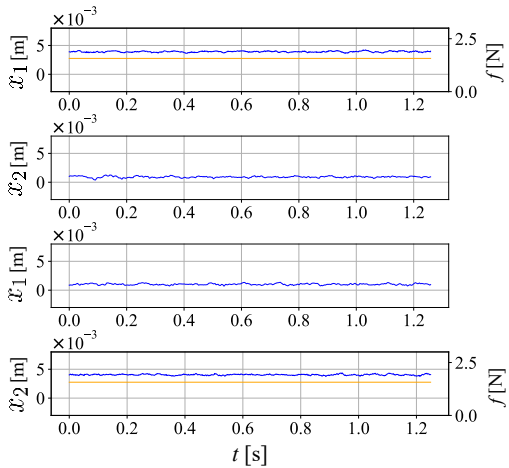


Fig10. Static measurement data of displacement (blue line) and force(orange line) for three spring model.

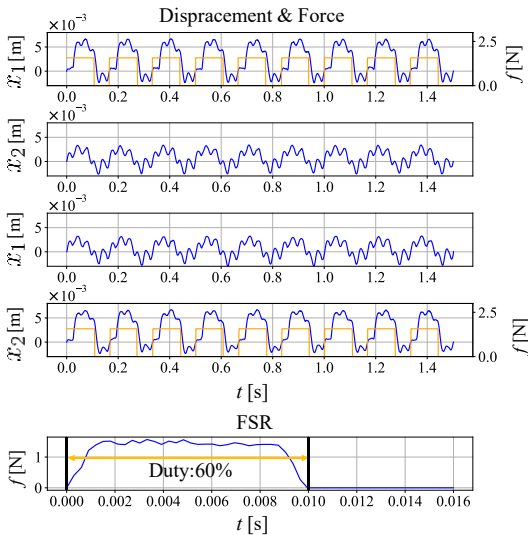


Fig 11. Dynamic measurement data of displacement (blue line) and force(orange line) in a two-spring model.

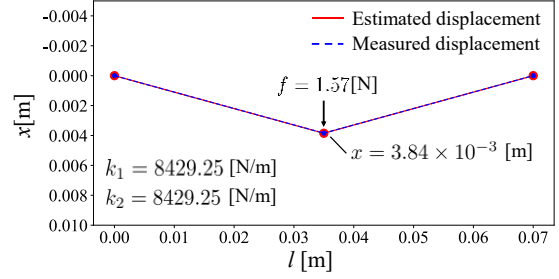


Fig12. Estimation results for a two-spring model. (when the force is static)

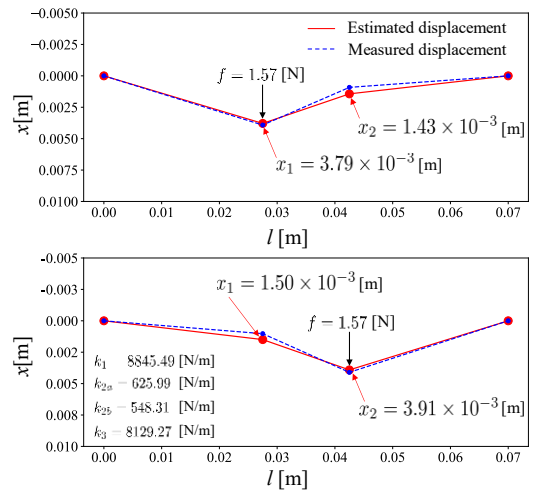


Fig13. Estimation results for three-spring models. The upper and lower figures show the static case with force applied to x_1 and x_2 , respectively

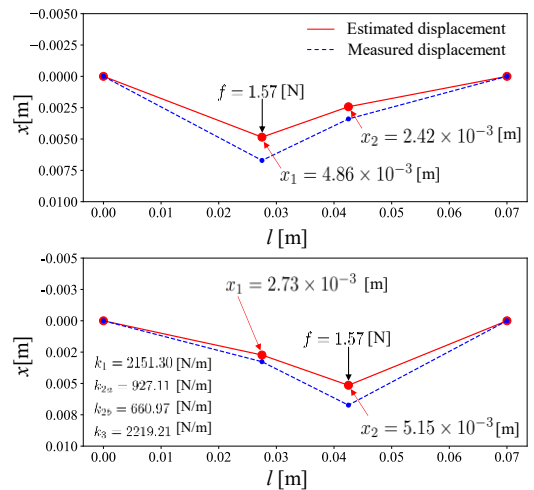


Fig14. Estimation results for the three springs model. The upper and lower figures show the case where the force is applied to x_1 and x_2 , respectively, where the force is dynamic.

References

1. I. Kato, K. Koganezawa, and A. Takanishi. Automatic breast cancer palpation robot:Wapro-4. *Advanced Robotics*, Vol. 3, No. 4, pp. 251–261, 1988.
2. P. S. Wellman and R. D. Howe. Modeling probe and tissue interaction for tumor feature extraction. In *1997 ASME Summer Bioengineering Conf.*, Vol. 35, pp. 237–238, 1997.
3. A. M. Galea and R. D. Howe. Mammography registered tactile imaging. *Surgery Simulation and Soft Tissue Modeling*, pp. 183–193, 2003.
4. M. B. Shields. Diagnostic and surgical techniques. *Survey of Ophthalmology*, Vol. 24, No. 4, pp. 211–219, 1980.
5. T. Kawahara, C. Toya, N. Tanaka, M. Kaneko, Y. Miyata, M. Okajima, and T. Asahara. Non-contact impedance imager with phase differentiator. In *Proc. of the 1st IEEE/RAS-EMBS Int. Conf. on Biomedical Robotics and Biomechatronics (BioRob2006)*, No. 159, 2006.
6. Y. Murayama, M. Haruta, Y. Hatakeyama, T. Shiina, H. Sakumab, S. Takenoshita, S. Omata, and C. E. Constantinou. Development of a new instrument for examination of stiffness in the breast using haptic sensor technology. *Sensors and Actuators, A: Physical*, Vol.143, No. 2, pp. 430–438, 2008.
7. C. Kleesattel and G. M. L. Gladwell. The contact-impedance meter-1. *ULTRASONICS*, Vol.6, pp.175–180, 7 1968.
8. H. L. Oestreicher. Field and impedance of an oscillating sphere in a viscoelastic medium with an application to biophysics. *The Journal of Acoustical Society of America*, Vol.23, No.6, pp.707–714, 1951.
9. G. M. L. Gladwell and C. Kleesattel. The contact-impedance meter-2. *ULTRASONICS*, Vol.6, No.4, pp.244–251, 10, 1968.
10. S. Omata and Y. Terunuma. New tactile sensor like the human hand and its applications. *Sensors and Actuators A*, Vol.35, pp.9–15, 1992.
11. S. Chen, M. Fatemi, J. F. Greenleaf, and Mayo Clinic. Shear property characterization of viscoelastic media using vibrations induced by ultrasound radiation force. *Proc IEEE Ultrason Symp*, Vol.2, pp.1871–1875, 2002.
12. M. Ochi, J. Iwasa, M. Tobita, M. Katoh, T. Yamamoto, R. Fukushima, and T. Kurushima. Method for measuring stiffness of a cultured tissue, using a stiffness measurement device having a vibration detective unit. *US Patent 7,198,908 B2*, 2007.
13. M. Kaneko, C. Toya and M. Okajima: Active Strobe Imager for Visualizing Dynamic Behavior of Tumors, *Proc.of the 2007 IEEE International Conf. on Robotics and Automation*, 3009/3014 (2007)
14. N. Tanaka and M. Kaneko: Skin Surface Shock Wave, *Proc. of Engineering in Medicine and Biology Society*, 2006. *EMBS '06. 28th Annual International Conference of the IEEE*, 4123/4126 (2006)
15. T. Kawahara, S. Matsunaga, S. Tanaka and M. kaneko: Non-contact Stiffness Imager, *Robotics Society of Japan*, Vol.24 No.3, pp.363-369, 2006.
16. K. Funai, K. Mizoue, M. Higashimori and M. Kaneko. Optimal Parameter Determination of Active Strobe Imager, *T. SICE Vol.46 No.12 December* (2010)
17. N. Tanaka, M. Higashimori, M. Kaneko, " Active Sensing for Viscoelastic Tissue with Coupling Effect", *SICE Journal of Control, Measurement, and System Integration*, Vol.44, No.10, 779-785, 2008.

Authors Introduction

Mr. Taiki Yamaguchi



He received his Master's degree from the Graduate School of Science and Engineering, Saga University, Japan, in 2022. He is currently a Doctoral course student at the Graduate School of Engineering Science, Osaka University, Japan.

Prof. Kensuke Harada



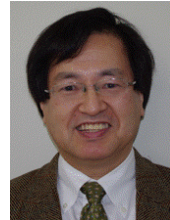
He is a Professor at the Graduate School of Engineering Science, Osaka University, Japan, a Fellow of the IEEE, and a Cross-Appointment Fellow at the National Institute of Advanced Industrial Science and Technology (AIST), Japan.

Mr. Kouji Mizoue



He completed his graduate studies in the Department of Electronic and Electrical Engineering at the Graduate School of Engineering, Fukuyama University, in 2001. He is the President of Mizoue Project Japan and is engaged in the production and development of medical measurement devices.

Prof. Makoto Kaneko



He is a Professor Emeritus at the Graduate School of Engineering, Osaka University, Japan. Currently, he serves as a Visiting Professor and is recognized as a Fellow of the IEEE.
